International Journal of Frontiers in
Chemistry and Pharmacy Research
Journal homepage: https://frontiersrj.com/journals/ijfcpr/
ISSN: 2783-0462 (Online)

(RESEARCH ARTICLE)

Synthesis and study the crystal structure of polycrystalline a novel type phase in Zn-Pb- Zr intermetallic alloy by ab initio method via powder XRD system

Janak Adhikari [1], Hareram Mishra [2] and Parashuram Mishra [1,*]

[1] *Bioinorganic and Materials Science Chemistry Research Lab, Tribhuvan University, M.M.A.M. Campus, Biratnagar, Nepal.*
[2] *Department of Physics, R.R.M. Campus, Tribhuvan University, Janakpurdham, Nepal.*

International Journal of Frontiers in Chemistry and Pharmacy Research, 2021, 01(01), 021–030

Publication history**:** Received on 26 February 2021; revised on 02 April 2021; accepted on 06 April 2021

Abstract

Zn- Pb- Zr ternary intermetallic phases were synthesized by high-temperature solid-state synthesis. Structural characterization was performed by means of powder X-ray diffraction and energy dispersive X-ray analysis. X-ray powder diffraction coupled with Rietveld refinement reveals the sample's phase purity we have prepared. Thermal behavior analysis shows $Zn_{0.61}$ $Pb_{0.91}$ $Zr_{0.138}$ is very stable, it doesn't decomposition until heated up to 998 °C. UV-visible absorption and diffuse reflection spectrum feature characteristic absorption bands of d-electron transition and main group metallic alloy given an optical band gap value of 3.65 eV. Magnetic susceptibilities measurement gives significant anti- ferromagnetic interactions between magnetic centers. The results further encourage the prospects of ternary Zn-Pb-Zr alloy anodes to utilize in real energy storage applications The photo degradation experiment were performed to evaluate photocatalytic activities of Zn0.61 Pb0.91 Zr0.138 .The Rietveld refinement parameters are a=8.731(Å),b=8.734(Å),c=5.929(Å), GOF=1.214,Rwp=31.21,Rp=21.321 having hexagonal crystal system with primitive . P 63/m c m space group.

Keywords: Novel; Magnetic; Transition; Antiferromagnetic; Photo degradation; Hexagonal

1. Introduction

Intermetallics are of great interest as they have a wide range of applications based on their electronic, optical, mechanical, and chemical properties. Their huge potential as heterogeneous catalyst thermoelectric materials magnetic materials semi and superconducting materials spintronics corrosion-resistant materials, energy storage materials are well investigated [1,2]. Atomic ordering, an integral characteristic for intermetallic phases, differentiates them from common alloys. They build their crystalline ordered structure where the positions of two (or more) types of atoms are defined, not random. Though most of the conventional molecules are fully ordered and stoichiometric in nature, sometimes intermetallics are not perfectly stoichiometric; bears defects and disorders. Many attractive properties have shown a strong correlation with atomic ordering in the crystal structure of the intermetallic compounds [3], Zn- Pb- Zr alloys (brasses) show a number of industrial applications. Mechanical and physical properties of brasses can be improved with the addition of a third element, for example, Pb (lead brasses) and Zr(zirconium brasses) [4]. Zn- Pb- Zr intermetallic alloy Zn-based materials have been proposed as one of the most promising anode materials in substitute of the graphite [5], due to their high packing density, high capacity and safe thermodynamic potentials. Large volume change in metallic Zn-anodes during charge reaction limits them from practical applications despite the advantages. Intermetallic alloy anodes can successfully lower the volume change upon alkali-ion interaction [6-9]. Therefore, a variety of binary and ternary Zn-based intermetallic anodes have been explored so far. Pb-Zr-Zn based ternary intermetallic compounds are highly stable at room temperature and have extensively been investigated as anode materials for rechargeable Li and Na-ion batteries. The alloying of Zn with Li and Na-ion proceeds via multiphase transformations and eventually results in the fully alkylated phase of Sn, i.e., Li22Sn5 and Na15Sn4 respectively [10-12]. In the course of multi-phase transitions, multiple electrontransfer added in excellent charge storage for

*Corresponding author: Parashuram Mishra
Bioinorganic and Materials Science Chemistry Research Lab,Tribhuvan University,M.M.A.M.Campus,Biratnagar,Nepal.

rechargeable Li and Na-ion batteries. Electrochemical performances of Li and Na-ion batteries can further be improved by incorporation of a third element (active or inactive for Li or Na-ion storage) into the ternary Zn- Pb- Zr containing alloys. This study aimed to investigate the Pb-Zr-Zn system as very few reports are available on Zn- Pb- Zr system [13]. Moreover, the literature was limited to the specific characteristics of compounds with a lack of valid crystallographic data. The use of the so-called "alloy-chemistry" methods permits not only to use energy-saving synthetic procedures but represents sometimes an only approach to metastable and/or kinetically hindered compounds. While exchange reactions in solution or between a solid phase and solution or melt are well known, the benefits of the solid-state exchange processes have been understood several decades ago. As in solution, this approach utilizes the assembly of various structural "building blocks" which are believed to be transferred from various solid precursors into the structure of the target solid product. This approach has been successfully applied to layered structures which opened the possibilities of constructing highlyordered 3D structures due to coalescence of the 2D building blocks [14]. The other perspective is that these reactions permit to change the contents of the interlayer space, particularly via introducing there various thermally or chemically unstable species when it is not possible via solution or ceramic routes (and references therein) [15]. Recently, we applied this approach to the synthesis of several layered compounds of transition and non-transition namely their oxide chromates and carbonates, via simple exchange reactions between LnOCl oxychlorides and potassium chromates and carbonates, respectively [16]. Contrary to the high-pressure synthesis of Pb-Zr-Zn or time-consuming low-temperature oxidation of format melts yielding intemetallic alloy, Pb-Zr-Zn the solid-state exchange reactions readily proceed at 400-900oC within several days yielding single-phase target compounds with the only by-product, KCl, easily washed out, commonly by water. This approach also permitted easy preparation of new type o alloy.Metal alloy compounds containing zirconium elements have greatly attract significant interest for their technologically important applications in many different fields, such as laser pumping, frequency conversion, photo luminescence, magnetic materials, and scintillator crystals.[17] In order to explore new materials with unique performances, different cations of different group elements have been introduced and combined with zirconium led to a variety of new framework materials, such as zinc silicates and lead zirconate ions . Although both sets of compounds exhibit high thermal stability and interesting optical and magnetic properties, compared with zinc silicates, germanate analogs are less investigated. For the ternary zinc- zirconate, some reported compounds feature interesting properties for potential applications. For example, apatite-type La9.33Ge6O26 single crystal works as an oxide ionic conductor,[18] Ho2Ge2O7 shows significantly anisotropic magnetic properties, and Eu2GeO5 exhibits strong red light emission.. Quaternary lanthanide germinates greatly increase the opportunities of performance modifications by introducing a more diverse set of atoms with differing radii and electronegativity. For example, La2MgGeO6 features a perovskite structure which is very scarce in Ge based compounds.[19] YFeGe2O7 exhibits a remarkable low-temperature ferromagnetic ordering phenomenon. Our previously work Eu2GeB2O8 shows a strong red emission.[20] In alkali metal lanthanide germinate system, most reported compounds are based on sodium cations.[21] Compounds with other cations are surprisingly limited.. We deem transition metal ions having mixed valence metal template cations with different radii may lead to new zinc, Pb and zirconium alloy with different frameworks and physical properties. Our research efforts in this field led to the discovery of Zn0.61 Pb0.91 Zr0.138 alloy and study the structure of new metal alloy. Herein, we reported its synthesis, crystal structure, and physical properties, by ab initio method via powder XRD.

2. Material and methods

All chemicals used were analytical grade. A polycrystalline sample of Zn0.61 Pb0.91 Zr0.138 alloy was synthesized by a standard solid state reaction using a mixture of high purity reagents of Zn, Pb and Zr as the starting materials in the molar ratio of 4: 4: 1 at high temperature. Ternary intermetallic at high-temperature solid-state synthesis. Highly purePb (shot, 99.999%, Alfa Aesar), Zn (teardrop-shot, mm,99.999%, Alfa Aesar) and Zr (shot, 6 mm, 99.999%, Alfa Aesar) were taken inside a quartz tube (diameter of 8 mm) according to their weight calculated from the nominal composition (in 300 mg scale). Then the tube was sealed under a high vacuum (~10_5 mbar) using a sealing unit equipped with a diffusion pump. The sealed ampoule (length 3 cm) was kept in a programmable chamber furnace (Ants 1200 ^{o}C muffle furnace). Initially, the ampoule was heated up to 500^{o}C by fast heating (120^{o}C/h), and the temperature dwelled for 24 h. The reaction mixture was then again heated to 850 ^{o}C with 12^{o}C/h ramping rate and hold at that temperature for 24 h for homogenizing the metal mixture. After that, the temperature was slowly (12 °C/h) reduced to 450 °Cand annealed at that temperature for the duration of 84 h. Finally, the furnace was again cooled down to 250^{o}C with a ramping rate of 10^{o}/h, and it was turned off to allow the ampoule for air cooling. A series of samples were prepared with a varied composition of Pb, Zn, and Zr using the previously mentioned temperature program to check the phase purity and determine the homogeneity range. Ingots obtained were brittle in nature with a silvery metallic luster and stable in air and water at room temperature.

3. Powder X-ray diffraction (PXRD) and refinement

PXRD was used for checking phase purity and phase detection. Room temperature (298 K) PXRD data were collected in a Rigaku fifth generation (Gen 5) MiniFlex600 desktop X-ray diffractometer, with the HyPix-400 MF 2D hybrid pixel array detector (HPAD) equipped with Cu Ka radiation (1.5418 Å). A Bruker D2 Phaser XRD with LYNXEYE XE-T detector was used for some PXRD experiments. All the diffraction patterns were recorded over 2θ range20-90° with a step size 0.02_. Rietveld refinements were carried out using JANA 2006 program and refinement spectra shown in figure 1.. 15th order Legendre polynomials were used to fit the background and the zero point error was refined freely. Reflections were fitted with the Pseudo-Voigt function (peak-shape function: GW, LX, LY; cutoff: 12). Peak asymmetry corrections were done when it was relevant. Refining the profile parameters, profile fit was achieved and to determine the phase purity of the compounds Rietveld refinement was performed figure2. Positional parameters of the structural model obtained from the powder X-ray diffraction data analysis (Table 2) were used as starting parameters for the refinement against the X-ray powder data collected for bulk samples and the crystallographic data shown in table 1.. All cell parameters and atom positions were refined. Displacement parameters were refined whenever possible.The full pattern is fitting and peak decomposition in the space group P 63/m c m using check cell program. Crystal structures. High-resolution data set was collected for Zn-Pb-Zr on a RigakuUltima IV diffractometer utilizing CuKα1,2 radiation. The refinement was done using the JANA2006 software indexing the powder patters was not straightforward as two sets of Miller indices are possible for the strongest reflections yielding two alternative unit cells which led to close residuals upon LeBail full-pattern decomposition. Subsequent Rietveld refinements clearly ruled out one of these due to intolerably dissimilar Zn-Zr distances in the Pb ions.. Final Rietveld refinement plot for for cited alloy is given in Fig. 1; general projection of the crystal structure is shown in figure. 2; The structural parameters were refined by the Reitveld method using the JANA program which gave GOF=1.214,Rwp=31.21,Rp=21.321. The density is determined by Archimedes principle.

4. Results and discussion

4.1. Structure determination and refinement

Our studies have confirmed the existence and the proposed crystal structure of alloy of Zn0.61 Pb0.91 Zr0.138 advantage of the double exchange method in the preparation of single-phase specimens.The g-brass type phases in Zn-Pb-Zr system exist with a significant homogeneity range. Several crystals from different regions were selected to understand the atomic arrangement of the three elements throughout the homogeneity range. The diffraction spots from powder crystal data were indexed in primitive hexagonal crystal system with the Laue group m3m. The non-centrosymmetric space group P 63/m c m (193) was chosen based on the Laue symmetry and condition of systematic absences. For all the specimens, structure solution was carried out using Superflip employed in JANA 2006. Initial structure solution of the powder crystal obtained from Zn0.61 Pb0.91 Zr0.138 data resulted independent atomic sites, M01 (4e), M02 (4e), M03 (6f), M04 (12i), M11 (4e), M12 (4e), M13 (6g) and M14 (12i). Herein, Pb and zinc sites were difficult to distinguish due to their similar scattering power of X-ray. As the phase was Zn-rich, initially, all the sites were assigned as zinc and refinement resulted in residual value Robs (F2) of 11.10%. According to this assignment, the M14 (12i) site showed a negative isotropic displacement parameter (Uiso ¼ _0.0070 Å2), which indicated the presence of heavier element (Pb). In the literature, many cP g-type phases (cP52; P43m; 215) are reported with the composition N9M4 (such as Zn9Al4, Zn9In4, Ag9In4, Pb9In4, Cu9Ga4). Their structure can be viewed as two topologically similar but compositionally different 26-atom g-clusters (A - N22M4 and B - N14M12). Clusters are arranged at high symmetry points (0, 0, 0) and (½, ½, ½) of hexagonal cage NO15P23 type unit cell. In N9M4, the larger atomic species, M occupy inner octahedral site of the A cluster and hexaoctahedral(CO) site of the B cluster to avoid or minimize the number of homoatomic contacts (M-M) between the large atoms. The atomic % of Pb-Zn - Zr) is 78:32 in Zn0.61 Pb0.91 Zr0.138 is close to the atomic % of N:M in N9M4 (69:31). Based on the occupancy of larger atoms in previously known cP g-phases, the IT site (M01) of the A cluster and CO site (M14) of the B cluster were initially assigned to Zn atoms in Zn0.61 Pb0.91 Zr0.138 and the model was refined (Robs (F2) ¼ 10.51%). At this stage, M14 (12i) site still showed a negative isotropic displacement parameter (Uiso 0.0049 Å2). Independent refinement of site occupancy factor exceeded unity (~1.315), which indicated the possibility of Zn mixing in this site. Thus, M14 site was refined as mixed Zn and Zr. A significant decrease in residual value Robs (F2) of 7.63% was observed, and the resulting composition was Zn0.61 Pb0.91 Zr0.138 .M13 (6g) site also showed a negative isotropic displacement parameter (Uiso ¼_0.0024 Å2), and independent site occupancy refinement exceeded unity (1.1173), which also indicated the possibility of Sn mixing in this site. Refinement of M13 site as a mixture of Zn and Zr resulted a composition Zn0.61 Pb0.91 Zr0.138 and residual value Robs (F2) of 7.20%. Finally, all atoms were refined anisotropically; followed by isotropic extinction correction was performed to complete the model. It results a small change in Zn zirconium and atomic percentage with a composition $Zn_{0.61}$ $Pb_{0.91}$ $Zr_{0.138}$, and residual value Robs (F2) of 2.94%. To attain agreement of refined composition with

the composition, M01 site (previously assigned as Zn) was mixed with Pb as independent site occupancy refinement of M01 site exceeded unity (1.052). The model renders Robs (F2) = 2.87% and GOF =1.35. The resulting composition $Zn_{0.61}$ $Pb_{0.91}$ $Zr_{0.138}$ obtained from the refinement fits well with the composition of the sample. This model was used for initial structural refinement for C1, C2, C3 and the refinement details are mentioned in Supporting Information (S1). For all samples, compositions obtained from powder XRD refinement agreed well with the atomic compositions from the XRD analysis. Crystallographic data details such as the refined atomic positions and equivalent isotropic displacement parameters are summarized in Table 2. A summary of loaded and refined composition obtained from powder crystal X-ray diffraction.

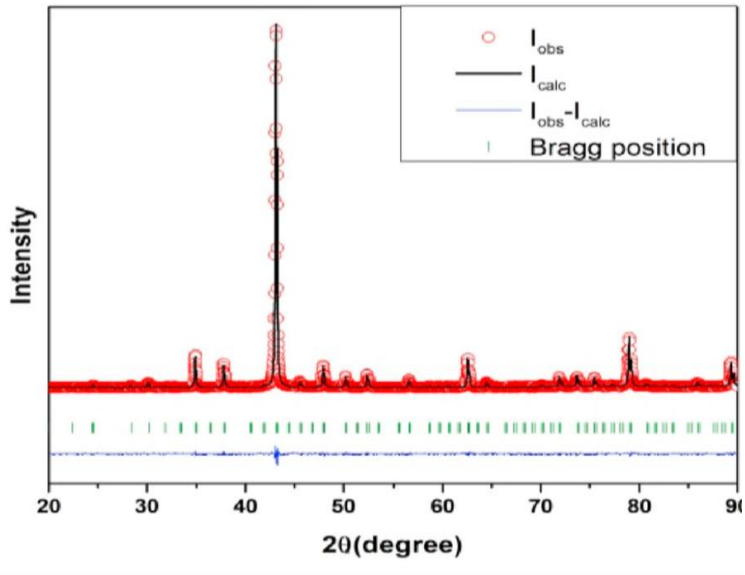

Figure1. Rietveld refinement of intermetallic alloy **$Zn_{0.61}$ $Pb_{0.91}$ $Zr_{0.138}$**

Table1 Crystallographic data of **$Zn_{0.61}$ $Pb_{0.91}$ $Zr_{0.138}$**

Formula sum	$Zn_{0.61}$ $Pb_{0.91}$ $Zr_{0.138}$
Formula weight	242.658 g/mol
Crystal system	hexagonal
Space-group	P 63/m c m (193)
Cell parameters	a=8.7341(7) Å,b=8.734(A) c=5.929(1) Å
Cell ratio	a/b=1.0000 b/c=1.4731 c/a=0.6788
Cell volume	391.70(9) $Å^3$
Z	2
Calc. density	1.3408 g/cm^3
Meas. density	1.5123g/cm^3
Index	0≤h≤1,-2≤k≤3,0≤l≤6
Pearson code	hP234
Formula type	NO15P23
Wyckoff sequence	h6g26ed6b

Table 2 Fraction Atomic parameters

Atom	Ox.	Wyck.	Site	x/a	y/b	z/c
Zn1	+2	2b	-3.m	0	0	0
Pb1	+2	6g	m2m	0.6157(1)	0	1/4
Zr2	+4	6g	m2m	0.2681(3)	0	1/4
Zr1	+4	4d	3.2	2/3	1/3	1/2
Zn1	+4	2b	-3.m	0	0	1/2
Pb1	+2	6g	m2m	-0.6157(1)	-0.6157(1)	1/4
Zr2	+4	6g	m2m	-0.2681(3)	-0.2681(3)	1/4
Zn2	+2	4d	3.2	-2/3	-1/3	0
Zr1	+4	4d	3.2	1/3	-1/3	0
Pb1	+2	6g	m2m	0	0.6157(1)	1/4
Zn2	+2	6g	m2m	0	0.2681(3)	1/4
Zn1	+2	4d	3.2	1/3	2/3	0
Zr1	+4	4d	3.2	-1/3	-2/3	0
Pb2	+2	4d	3.2	-1/3	1/3	0
Zn3	+2	4d	3.2	2/3	1/3	0
Zr1	+4	4d	3.2	-2/3	-1/3	1/2
Zr1	+4	4d	3.2	1/3	-1/3	1/2
Zr1	+4	4d	3.2	1/3	2/3	1/2
Zr1	+4	4d	3.2	-1/3	-2/3	1/2
Pb1	+2	6g	m2m	0.00000	0.3843(1)	3/4
Zr2	+4	6g	m2m	-0.2681(3)	0.7319(3)	1/4
Zr2	+4	6g	m2m	0.7319(3)	-0.2681(3)	1/4

4.2. Phase analysis

The details phase analysis of g-brass type Zn- Pb- Zrsystem was carried out by means of preparative methods, X-ray diffraction, and EDX analysis. Initial effort to synthesize $Zn_{0.61}$ $Pb_{0.91}$ $Zr_{0.138}$ (x ¼ 0, 0.5, 1.0) resulted g-brass type Zn- Pb- Zr ternary compounds as major phases. A large number of samples were synthesized based on the initial phase analysis. Powder ZRD crystal refinement agree well and confirmed the existence of an extended homogeneity range. The loaded compositions and their corresponding products, as identified by Xray powder diffraction shows Rietveld refinement plots for PXRD data of the four samples in figure 1.A systematic synthetic exploration of the Zn- Pb- Zr system confirmed that phase pure ternary compounds are formed for compositions ranging between 48 and 70 atomic % Zn, between 15 and 46 atomic % Zr, and between 5 and 15 atomic % Pb. Beyond the homogeneity range, secondary phases (such as Zr-Zn-Pb [P 63/m c m (193)], A partial phase triangle of the CueZneSn ternary system was drawn based on loaded compositions and shown in Fig. 3. Our attempt to prepare Sn substituted g-Zn5Zr8 with the loaded compositions Zn3.8Zr6.2-xPbx (x ¼ 0.5, 1.0, 1.5) produced the Zn-rich g-brass type compound as major phase and b-Pb coexisted with the main phase shown in figure 3 . Partial substitution of bivalent zinc bytetravalent tin in g-Zr5Zn8, pushes VEC value away from the stability range for g-brasses (1.56-1.70 e/a). Hence, Zn insertion at the Zn site may drive a simultaneous increase of monovalent Cu by the reduction of Zn in Zn- Pb- Zr ternary phases to keep the VEC in the range where gbrasses exist. As a consequence, g-brass type Cu-rich phases are formed in the Zn- Pb- Zr system. VEC of g-brass type Zn- Pb- Zr phases are calculated based on both loaded composition and PXRD refined composition, and it is found that e/a varies.

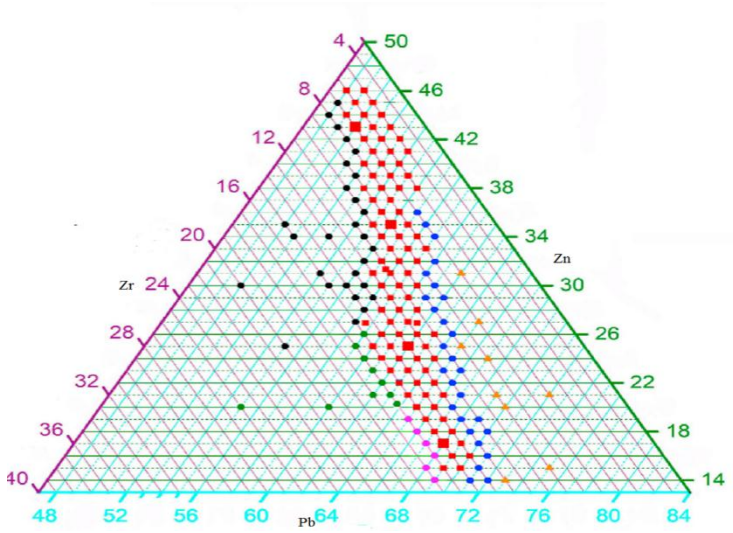

Figure 2. Partial phase triangle of the Zn-Zr-Pb system at 450°C based on the starting composition

4.3. Structural description

The ternary g-brass type phases in the Zn- Pb- Zr system crystallizes in the a centric space group P 63/m c m (193)with 42 atoms in the hexagonal unit cell that are distributed over eight crystallographically independent positions depending on the chemical composition of the phase. The Zn- Pb- Zr alloy g-brass cage type structures consist of two compositionally different g-clusters in a primitive hexagonal unit cell with their vacant centers located at (0, 0, 0) and (½, ½, ½) positions of the hexagonal cells shown in figure 2. Decoration of atoms in the polyhedral shell of the g-clusters in the ternary g-phases is listed in Table 4 The g-brass cluster at (0, 0, 0) site is Curich, chemically more ordered than the cluster present at (½, ½, ½) 5 In the g-brass cluster at (0, 0, 0), OT, OH, CO sites are exclusively occupied by Zn throughout the entire homogeneity range. Only the IT site is mixed (Zn/Zr) and majorly occupied by Zn atoms. Zr content at this site ranges between 0.5 and 2 atomic %. The cluster is chemically more or less ordered with a composition ~ Zn8Zr4, though fully ordered Zr-free g-cluster is not found at (0, 0, 0) in the region of our investigation. The g-brass cluster at (½, ½, ½) is heavily disordered. Only the OT site is exclusively occupied by Cu all over the phase region. For Zn rich samples IT site is fully occupied by Zn, and with increase of Cu content it is mixed occupied between Pb and Zn, and completely occupied by Pb at Pb-rich side of the Zn- Pb- Zr phases. OH site is fully occupied by Zn at Zn rich side. The same site is mixed occupied between Cu, Zn andPb for the composition at intermediate Zn-concentration and Zn/Pb at Zn poor side. CO site of B cluster is occupied by Zn and Zr. Majority of Pb goes to this particular site.Pb concentration at CO site (~6 at. % - ~12 at. %) increases with overall Pb content (~6 at. % -~14 at. %) in the ternary phases. At a fixed Sn concentration, if the ratio of Zr-Zn increases in the Zn-Pb-Zr phases, occupancy of Zr at IT site (Zn01/Pb0.2) of cluster A (0, 0, 0) gradually decreases with the simultaneous increase of Sn at OH site of cluster B (½, ½, ½), whereas the occupancy factor of Zn remains more or less same at CO site of the B cluster. The variation ofZr:Zn ratio in the ternary phases is associated with the change of site occupancy factors of Pb//Zn at OH site of cluster B (½, ½, ½) were cycled within the voltage range of 0.005e2 V at a current rate of 0.2C. On moving from $Zn_{0.61}$ $Pb_{0.91}$ $Zr_{0.138}$ the chemical composition shows a decrease in Zn atoms and an increase in Zn, Zr and Pb atoms. Zr-atom remains electrochemically inactive to lithium and sodium. The electrochemically active species which take part in the alloying/de-alloying are Zn and Zr at various stoichiometry. The theoretical capacities for the electrode materials were calculated based on alloying/de-alloying activity of electrochemically active Zn and Sn with alkali metal-ion (Li and Na). During alloying/de-alloying process, one electron transfer has been taken into consideration complementing 1 mol of alkali ion transfer into the ternary intermetallic material. By Faraday's law, the theoretical capacities of $Zn_{0.61}$ $Pb_{0.91}$ $Zr_{0.138}$ (C1 as 169.6, 135.4, 94.1 and 92.7 mAhg_1 respectively In the first discharge cycle of $Zn_{0.61}$ $Pb_{0.91}$ $Zr_{0.138}$ electrode, a sloping voltage line from 1.6 to 1.0 V and four alloying peaks are noticeable at 0.75, 0.39 and 0.13 and < 0.1 V No distinctive potential peak in between 1.6 and 1.0 V regions indicates the SEI formation due to electrolyte decomposition. As reported by literature, a wide range of binary phases of Zr/Pb (M ¼ Zn).The structure of of cited alloy shown in figure 3.

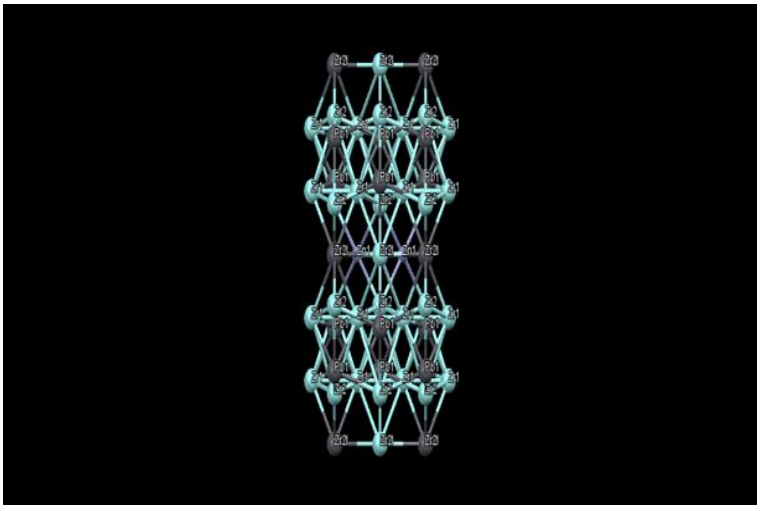

Figure 3. 3D structure of $Zn_{0.61}$ $Pb_{0.91}$ $Zr_{0.138}$

4.4. Electrochemistry

Electrochemical alloying of metals during Li-ion intercalation proceed via various voltage plateau indicating Li-poor, medium and rich phases of LixMy. The voltage plateau at 0.75 V in Fig. 5a corresponds to the formation of Li-poor phase LiSn. The subsequent voltage plateau at 0.39 V can be addressed to Li-rich phases, such as Li7Sn3, Li5Sn2, Li13Sn5, and LiZn. In our opinion, this short plateau at 0.39 V appears due to Zn-alloying of Li-ion. However, we have considered this voltage as the starting point for Zn-alloying of Ni ions. Following this, a less intense peak at 0.13 V has been observed on the first two cycles of the differential capacity plot which confirms the activity of Zn-alloying. The peak at 0.13 V elucidates the fully lithiated phase of Pb/Zn. As we move towards less Zn-atom containing ternary intermetallics, the plateau at 0.39 V starts weakening and eventually disappears for the Zr rich compounds Zn0.61 Pb0.91 Zr0.138 Similar behavior has been observed for the peak at 0.13 V, which corroborates the Zn-alloying mechanism of Zn-ion in the ternary intermetallic compounds. The sharp peak emerging below 100 mV reveals the formation of a fully lithiated phase of Zn/Zr . In the subsequent discharge cycles, the disappearance of Li-poor Zn-alloying peak (at 0.75 V) and a continuous fading of Zn-alloying peaks (at 0.39 and 0.13 V) have been observed. However, upon further cycling, a complete reversible alloying/dealloying mechanism has been identified with ~0.2 mol of Li-ion insertion/extraction. The reversible capacity is noted as~30 mAhg_1 at a high capacity rate of 0.2C with an average voltage of 250 mV after 20 cycles Upon electrochemical tests on Zn0.61 Pb0.91 Zr0.138a few changes in alloying/de-alloying mechanisms have been observed owing to decreasing Zn-content and increasing Zn,-Zr content. Zn0.61 Pb0.91 Zr0.138 electrode exerts two alloying peaks at 0.71 and 0.54 V in the first discharge cycle, as shown in Fig. 5d. As stated earlier, the sharp peak at 0.75 V corresponds to the formation of Lipoor compound Zn/Zr The broad peak at 0.52 V can be assigned to Zn-alloying during the initial Li-ion insertion reaction to form LiZn. Moreover, fully lithiated phase of $Li_{22}Sn_5$ surfaces at a peak potential below 100 mV. On the subsequent cycling, the Li-poor Snalloying peak disappears. As the voltage peak at ~0.1/0.2 V dominates in further cycling, it is predicted that the reversible alloying/de-alloying occurs only between Zn-rich phase of Zn/Pb and the inserted Zn-ion. Upon further increasing Zn content in $Zn_{0.61}$ $Pb_{0.91}$ $Zr_{0.138}$ no Zn-alloying peaks have been observed during initial Pb-ion insertion reaction .The sharp peak at 0.75 V becomes constant for all the samples showing a Li-poor binary phase formation as Li/Zn. In addition, the high intensity peak below 100mV ensures the formation of $Zn_{0.61}$ $Pb_{0.91}$ $Zr_{0.138}$ electrodes result a reversible capacity of ~20 and ~22 mAhg_1 respectively after 30 cycles similar galvanostatic charge-discharge studies have been approached to understand the electrochemical characteristics of ternary intermetallic compounds during Na-ion reaction. Although the Zn-ion insertion/extraction mechanism is found to be as similar as Ni-ion reaction, the positions of voltage plateau are altered.

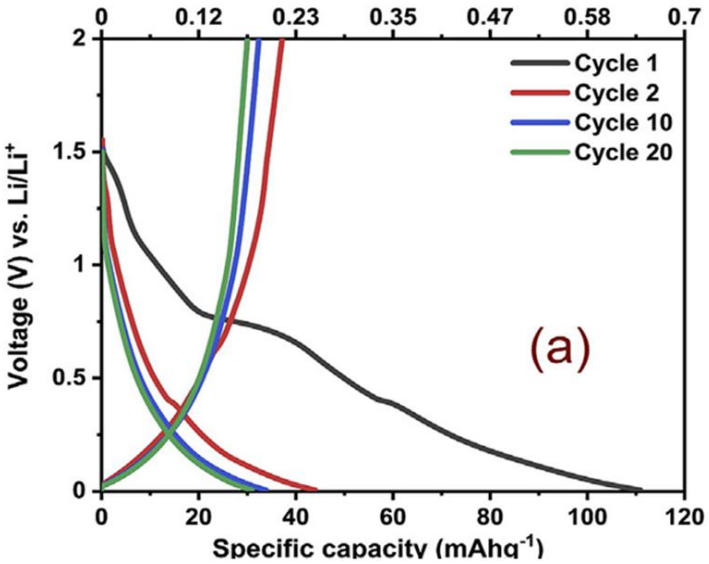

Figure 4. Charge-discharge profiles and Differential capacity plots of ternary intermetallic electrodes during Zn-ion reaction cycled at a rate as high as 0.2C between the voltage range of 0.005-2 V of $\mathbf{Zn_{0.61}\,Pb_{0.91}\,Zr_{0.138}}$

The chemical compositions of Zr and Zn-alloys of Na-ion are also different as compared to Li-systems. The initial Na-ion insertion capacities are found to be 79.9, 49.8, 39.7 and 57.5 mAhg-1 respectively, as shown in Fig. 5 .The initial discharge capacities execute similar trend as Li-ion systems. The alloying/de-alloying steps during Na-ion interaction have further been explained through differential capacity plots as shown in Figure 5.Therefore; the extensive galvanostatic studies suggest three factors which influence the electrochemical behavior of Zn-Zr-Pb samples during Li- and Na-ion reaction. First, all the intermetallic Zn-Zr-Pb samples experience large polarization during initial lithiation and sodiation. Such polarization is reflected in the differential capacity plots as the peak potentials are completely different in values in the first cycle than in the consecutive cycles. No significant change in peak potentials is observed after the initial cycle, which extends high reversibility of the charge-discharge process. Second, a limited number of alkali-ion insertions in the present study correspond to low volume expansion in the initial cycle on contrary to pure metal anodes. A large number of initial Li and Na-ion insertions (4.4 and 3.75 mol respectively) in pure Zn metal anodes cause high volume expansion, thus worsening their electrochemical performances. Therefore, restricted alkali-ion insertion improves the cycle stability of the $Zn_{0.61}$ $Pb_{0.91}$ $Zr_{0.138}$ electrodes. Third, excess Zn -atoms in Zn-Zr-Pb intermetallics can provide a buffer layer to withstand the mechanical stress during volume change. Excess Zn-content assists in stable SEI formation, which furnishes high cycle stability after the initial cycle. An overall improvement in the second cycle discharge capacity retention has been observed in all the samples during both Li- and Na-ion reaction. In addition, more Zr-rich intermetallic Zn-Zr-Pb sample is found to alleviate the volume expansion to a greater extent performing better capacity retention from the second discharge cycle

5. Conclusion

New g-brass type $Zn_{0.61}$ $Pb_{0.91}$ $Zr_{0.138}$ intermetallic ternary compounds have been synthesized by conventional high-temperature solid-state method. Powder X-ray diffraction analysis indicates a site specific Zn substitution in the ternary g-brass ($Zn_{0.61}$ $Pb_{0.91}$ $Zr_{0.138}$) changes the atomic decoration in the 30-atom g-cluster, and it reduces the centering from cubic I to hexagonal structure. The structure of $Zn_{0.61}$ $Pb_{0.91}$ $Zr_{0.138}$ ternary g-brass was described by two topologically similar but compositionally different g-cluster in the primitive hexagonal unit cell. The Zn -rich g-cluster centered at (0, 0, 0) was chemically more ordered than the cluster present at (½, ½, ½). An extended phase width of the ternary compound was identified using X-ray analysis. Structures of several samples with different compositions were studied by X-ray using Rietveld refinement with Mercury and diamond software programme.A systematic variation of the constituent elements over different crystallographic sites was observed on moving from Zr to Zn -rich sample of the Zn-Zr-Pb phases. The compounds are stabilized between 1.57 and 1.70 e/a. The electrochemical performances of the samples was analysed for the application in rechargeable Li- and Na-ion batteries. A limited amount of alkaliion insertion/extraction rendered remarkable capacity retention at rapid charge-discharge cycling. Reduced stress due to low volume expansion, stable SEI formation and buffering of Zn-layers in Zn-rich Zn-Zr-Pb ternary intermetallics served superior charge capacity retention of above 80% during Li-ion reactions.The confirmation of structure was analysed by Rietveld refinement using Diamond computer programme and Mercury software programme.

In this way the prediction of the reaction pathway during the lithiation at room temperature using SbSn as anode material would be possible. Future large scale applications of $Zn_{0.61}$ $Pb_{0.91}$ $Zr_{0.138}$-anodes in galvanic cells are limited by relatively high costs of the materials and the discussion of declaring Pb as a toxic material which has to be largely banned from industrial productions. However, they are still interesting as niche products for special applications and also determined the structure of cited ternary alloy by ab initio method via powder XRD.

Compliance with ethical standards

Acknowledgments

The authors would like to acknowledge the immense contribution laboratory staff of Department of Chemistry University of Delhi,India for provide the XRD data

Disclosure of conflict of interest

The authors declare that they have no conflict of interest.

References

[1] L. Roffner, M Armbrüster(2019), Electrochemical energy conversion on intermetallic compounds: a review, ACS Catal. 9(3): 2018-2062.

[2] A Dasgupta, RM Rioux(2019),Intermetallics in catalysis: an exciting subset of Multimetallic catalysts, Catal. Today.30: 215-230.

[3] KF Liu, SQ Xia.(2019) Recent progresses on thermoelectric zintl phases: structures, materials and optimization, J. Solid State Chem. November , 270: 252-264.

[4] Y Xing, R Liu, J Liao, Q Zhang, X Xia, C Wang, H Huang, J Chu, M Gu, T Zhu, C Zhu, F Xu, D Yao, Y Zeng, S Bai, C Uher, L Chen.(2019) High-efficiency halfheusler thermoelectric Modules enabled by self-propagating Synthesis and topologic structure optimization, Energy Environ. Sci. 12(11): 3390-3399.

[5] YZhang.(2019) Review of the structural, magnetic and Magnetocaloric properties internary rare earth RE2T2X type intermetallic compounds, J. Alloys Compd. 787: 1173-1186.

[6] S Klenner, Z Zhang, R P€ottgen, L Li(2020), Magnetic and Magnetocaloric properties of the equiatomic europium intermetallicsEuAgZn, EuAgCd, EuPtZn and EuAuCd, Intermetallics. 120: 1-7.

[7] SA Khandy, I Islam, DC Gupta, R Khenata. ALaref. Lattice dynamics, mechanical stability and electronic structure of Fe-based heusler semiconductors, Sci. Rep. 2019; 9(1): 1-8.

[8] MS Likhanov, RA Khalaniya, VY Verchenko, AAGippius, SVZhurenko, AV Tkachev, DI Fazlizhanova, AN Kuznetsov, AV Shevelkov(2019), ReGaGe2: anintermetallic compound with semiconducting properties and localized bonding, Chem. Commun. 55(41): 5821-5824.

[9] VY Verchenko, AO Zubtsovskii, DSPlenkin, AV Bogach, Z Wei, AA Tsirlin, EV Dikarev, (2020), Family of Mo 4 Ga 21 -based superconductors, Chem. Mater. 32(15): 6730-6735.

[10] A Reigle, K Mason, J Slattery, S Lee, T Jamison, A Eggert, V Vincely, D Wong, YGuo, J Brock, M Khan.(2019) Superconducting properties of in doped ZrNi 2 Ga1_x in X, Solid State Commun. 291: 28-31.

[11] K Elphick, W Frost, M Samiepour, T Kubota, K Takanashi, S Hiroaki, S Mitani, AHirohata.Heusler(2020), Alloys for Spintronic Devices: Review on RecentDevelopment and Future Perspectives, Taylor & Francis.

[12] S Li, X Wang, Z Liu, Y Jiu, S Zhang, J Geng, X Chen, S Wu, P He, W Long.(2020) Corrosion behavior of Sn-based lead-free solder alloys: a review, J. Mater. Sci. Mater. Electron. 31(12): 9076-9090.

[13] MA Fazal, NK Liyana, S Rubaiee.A Anas.(2019), A critical review on performance,Microstructure and corrosion resistance of Pb-free solders, Meas. J. Int. Meas. Confed. 134: 897-907.

[14] Z Yi, Z Wang, Y Cheng, L Wang (2018).Sn-based intermetallic compounds for Li-ion batteries: structures, lithiation mechanism, and electrochemical performances, Energy Environ. Mater. 1(3): 132-147.

[15] W. Luo, J Gaumet, LQ Mai (2017). Antimony-based intermetallic compounds for lithium-ion and sodium-ion batteries: Synthesis, construction and application, Rare Met. 36(5): 321-338.

[16] Y Liu, L Wang, K Jiang, S Yang.(2019), Electro-deposition preparation of selfstanding Cu-Sn alloy anode electrode for lithium ion battery, J. AlloysCompd. 775-825.

[17] Samiran Misra , Deban jana Pahari , Souvik Giri , Sreeraj Puravankara , Partha P. Jana(2021), Synthesis, crystal structures, phase width and electrochemical performances of g-brass type phases in CueZneSn system, Journal of Alloys and Compounds. 855: 157372

[18] Martin Tsvetkov, Maria Milanova, bLaura C. J. Pereira,bJo˜ao C. Waerenborgh, Zara CherkezovZheleva, Joana Zahariev Ivan Mitov(2016), Magnetic properties of binary and ternary mixed metal oxides NiFe2O4 and Zn0.5Ni0.5Fe2O4 doped with rare earths by sol–gel synthesis, Chemical Papers 70 (12) 1600–1610 , DOI: 10.1515/chempap-2016-0097

[19] Bimal K. Kanth, Parashuram Mishra.(2020), Synthesis and Ab Initio Determination Bi1.256 La0.53 N0.231 O0.521 Zr1.543 Triclinic Structure from Powder X-Ray Diffraction Data, Scholars International Journal of Chemistry and Material Sciences. 3(6): 122-130.

[20] Yuv Raj Sahu, Parashuram Mishra.(2020) Morphology and Study the Crystal Chemistry of a Novel Ternary Mixed Valence Bi1.52 Co2.52 Zr0.751 N0.641 O8.12 Oxide Orthorhomic Crystal Structure by Ab Initio Method via Powder XRD. 2020; 3(7): 99-108.

[21] Patric Berger, Hans Flandorfer,(2021), Sb-Sn alloy anodes for Li-ion batteries: The ternary system Li-Sb-Sn, Journal of Alloys and Compounds 855 (2021) 157381.

[22] D. Li, A. Beutl, H Flandorfer, DM Cupid.(2017) The Li-Sb phase diagram part II: calorimetry and thermodynamic assessment, J. Alloys Compd. 701: 186-199.